03

# Model of jet plasma flow with absorption of a $CO_2$-laser pulse

© V.I. Yakovlev, T.A. Korotaeva

Khristianovich Institute of Theoretical and Applied Mechanics,
Siberian Branch, Russian Academy of Sciences, Novosibirsk, Russia
e-mail: yakovlvi@itam.nsc.ru

*Received April 22, 2024*
*Revised November 2, 2025*
*Accepted February 6, 2025*

An approach has been developed and numerical simulation of the dynamics of an optical discharge plasma has been carried out on the time scale of absorption of a $CO_2$-laser pulse. The features of the propagation modes of optical discharges are taken into account: light supported detonation wave (LSDW) and fast ionization wave. A system of hydrodynamic equations with energy sources is used, supplemented by the calculated value of the integral parameter the momentum caused by the microjet flow of the LSDW plasma. A comparison of the results of numerical modeling and visualization of plasma glow shows their close agreement when taking into account the microjet flow. Characteristic trends in the dynamics of the structure and parameters of the plasma in the microsecond range of the laser pulse are determined.

**Keywords:** optical discharge, light supported detonation wave, microjet flow, numerical modeling, plasma glow.

DOI: 10.61011/TP.2025.06.61370.141-24

## Introduction

The study of energy impact on gas flow is a promising area of research in the field of plasma aerodynamics [1]. Energy is carried by plasma of electric discharges of various types; plasma (pulsed, pulsating) of optical discharges is also used in conditions where it is required to supply and localize the energy in a gas flow by a non-contact method [2].

In many numerical studies the effect of laser plasma/flow interaction took place within a gas-dynamic model providing for the spatiotemporal distribution of the flow-absorbed energy — the energy source [3,4]. The correspondence of the calculated and experimental results was observed when the spatiotemporal parameters of laser plasma were exceeded due to the relatively rapid dissipation of absorbed energy in the medium. In case of a „point“ and extended focusing with a small diameter of laser beam, high consistency with the model of a point (spherical, cylindrical) explosion was observed [5]. However, in the specific spatiotemporal scale of a laser pulse, it is necessary to take into account the behavior pattern of the optical discharge plasma.

Laser plasma is formed in various modes of optical discharge propagation [6]; each corresponds to the dominant mechanism of plasma front transfer. The processes occurring in the front — heating, compression and expansion of gas, absorption of laser radiation, ionization relaxation, electronic thermal conductivity — determine its structure and propagation patterns depending on the parameters of the medium and intensity of laser radiation. Among the supersonic modes the laser-supported detonation wave (LSDW) is the most sophisticated one, since plasma front contains a step shock [7], however, along with that, this mode is the most common one [7] presents a computational and theoretical analysis of the structure and regularities of LSDW's plane front restructuring in hydrogen, helium, and argon at different intensities of $(q)$ laser radiation. At high intensity higher velocities may occur [8], e.g., radiation-induced (radiation wave) and fast ionization wave (FIW) due to the plasma radiation transfer. In the first mode the medium is ionized by UV plasma radiation; the second one differs in that FIW only „initiates“ the avalanche, while the energy necessary for gas ionization comes from the laser radiation [9]. The modes associated with plasma radiation transfer require a noticeable optical thickness of plasma layer in the laser beam, therefore, the area of their existence depends, among other things, on the beam radius $r$, which shall be higher than the critical value (at least $\sim 0.1$ mm). For this reason [8] it is stated that only LSDW mode is possible in case of a point beam focusing (small $r$). The analysis of physical models of optical discharge propagation modes obtained in [7–9] demonstrates, also as in experiments, high velocity of plasma front ($V \sim 10-100$ km/s). An exponential approximation as $V \propto q^a$ is observed, where $q$ — intensity, [W/cm$^2$], and $a$ — an experimentally found value which almost doesn't differ from the initial parameters and intensities. FIW is characterized by an indicator of $a > 1(2-3.5)$, while for other modes of plasma front propagation $1/3 < a < 1$ [10]. In particular, parameter $a = 1/3$ corresponds to LSDW [6].

Thus, the implementation of a particular mode significantly depends on the energy parameters of the laser beam and its focusing conditions, as well as the parameters of the medium. As a result, it is possible to transform the mode during the pulse duration, with a rapid increase in intensity and subsequent decrease at a slower rate. Thus, in the study [11,12] of laser plasma within the spatiotemporal scale of absorption of $CO_2$-laser beam it was found that

FIW at the peak pulse intensity transforms into a slower ($\leq 10$ km/s) LSDW mode when the ionization subsides. In the experiments [13,14], LSDW was observed even under short beam focusing, and then stopped due to heavy expansion of plasma. In contrast to [11,12], paper [15] describes for the peak intensity of laser pulse the LSDW transforming into FIW when the radiation „plateau“ is still quite high. Such an uncharacteristic sequence of discharge propagation modes is due to small diameter of the primary plasma, its subsequent expansion, and the absorption of radiation intensity „plateau“ that is still high enough for FIW. Here we may see the dependence of FIW mode on the focusing conditions.

Recently, there has been an increasing number of works with a detailed analysis of the processes of primary laser plasma formation at the stage of discharge front formation. For example, in [16], the fluid dynamics of a discharge in a short-wavelength laser beam (532 nm) is modeled on a nanosecond time scale. The Navier-Stokes equations are used taking into account chemical kinetics, as well as radiation transfer equations, including multiphoton ionization and reverse braking radiation. Energy absorption occurs through a mechanism that is the reverse of braking radiation, which compensates for the loss of free electron energy during cascade ionization. The modeling results demonstrated formation of plasma waves in both the forward and reverse directions with respect to the beam. The laser plasma transforms into a two-leaf structure with a good consistency between the axial and radial dimensions of plasma observed in the experiments. In fact, in this study, the role of breakdown mechanisms was determined for the initial stage of plasma front formation in one of the modes of discharge propagation on the nanosecond time scale typical of the short-wavelength lasers. However, examination of the later stage of the discharge propagation was not the objective of this study. At this stage, the scale of plasmodynamic processes significantly (by orders of magnitude) exceeds the nanosecond time scale of kinetic processes in plasma, which requires other modeling methods.

Determining the behavior of laser plasma in space-time scale of energy absorption is a relevant issue for plasma aerodynamics, the solution of which makes it possible to determine ways to control the aerodynamic characteristics of high-speed bodies [2]. For example, in [17], based on the model of non-viscous, perfect, equilibrium, radiating air, a numerical study of the gas-dynamic structures of plasma formations arising from the laser-supported detonation absorption of laser radiation near a body was performed. In addition to the system of equations of fluid dynamics, the radiation transfer equation was used in the diffusion approximation using the air absorption coefficient, which includes nine spectral intervals. The intensity and wavelength of laser radiation were taken as variable parameters. It is shown that at atmospheric pressure for laser emitters of different spectra, the relationship between their intensity and the propagation velocity of laser absorption waves remains the same ($V \propto q^a$, $a = 0.72$). It was also demonstrated that lower air density resulted in reduced gas compression in LSDW, and it degenerated into a radiation wave.

In paper [18] numerical modeling allowed to determine spatial distributions of parameters of the axisymmetric plasma downstream the front of stationary LSDW ($a = 1/3$) in a constant-diameter laser beam in the approximation of an infinitely subtle absorption front. A critical singularity of LSDW was found: downstream the front a micro-jet plasma flow is formed with a high velocity of up to 0.5 velocity of $V$ front towards the laser beam and having a cross-section of its several diameters. The interaction of a high-speed micro-jet with the external environment can determine the features of the discharge plasma dynamics in terms of laser pulse space and time, which differ from localized energy release without taking into account its formation. Therefore, high plasma velocity found in the experiments [15,19] downstream LSDW front at $CO_2$-laser absorption may be explained given the interaction of the micro-jet plasma flow with the external environment. In [20], it was first suggested that plasma downstream LSDW front acquires a quantity of motion in the direction of the laser beam — a LSDW pulse, i.e., an additional force exerted on the flow. A method for estimating the magnitude of a micro-jet pulse using an analytical method for calculating its parameters is briefly described [18]. The result is used to determine the structure of a supersonic flow with a pulsating laser plasma. A significant difference in the flow structure is shown when the micro-jet plasma flow emerges and when it is absent. However, the calculated amount of plasma LSDW motion used in [20] does not have sufficient justification based on a comprehensive analysis of experimental and calculated data.

The purpose of this work was to develop an approach and perform numerical modeling of laser plasma behavior, taking into account the modes of discharge propagation established in the experiment [15]. A comparative analysis of the results of numerical modeling and visualization of laser plasma luminescence on a typical time scale of laser pulse absorption $CO_2$-will allow testing the calculated value of the plasma shear pulse within the framework of the numerical model used.

Given the significance of the plasma pulse LSDW magnitude, section 1 provides a more extensive description of the parameter calculation method compared to [20] added with estimates of the approximations used.

## 1. Jet flow in LSDW mode

### 1.1. Plasma pulse calculation

To determine the jet plasma flow the data are used on distribution of the fluid dynamics parameters downstream LSDW front counter-running at a rate of $V$ in a laser beam $d_0 = 2r_0$ in diameter. Assuming, as established in [18], a fairly uniform distribution of parameters over the plasma jet section, we obtain that the pulse $P^*$ is equal to the value of

the integral defined within $x = 0 - x_0$:

$$P^* = \int \rho(x)u(x)\pi(r(x))^2 dx. \quad (1)$$

Here $x_0$ — length of LSDW plasma stretched along $OX$ axis; $\rho(x)$, $u(x)$ and $r(x)$ — axial distributions of density, relative velocity and radius of the jet flow; area of the jet cross-section — $\pi[r(x)]^2$.

Using the relative values of density $\rho/\rho_\infty$, velocity $u/V$, radius $r(x)/r_0$ and distance $z = x/d_0$, we get that expression for pulse (1) looks as

$$P^* = \int \rho(x)u(x)\pi(r(x))^2 dx$$

$$= \rho_\infty V(\pi r_0^2)d_0 \int \rho(z)u(z)(r(z)/r_0)^2 dz. \quad (2)$$

Accordingly, the value of specific (per unit volume) pulse $P$ is found from the expression

$$P = KP_o,\ K = \int \rho(z)u(z)(r(z)/r_0)^2 dz,\ P_0 = \rho_\infty V. \quad (3)$$

The calculation of $K$ coefficient, depending on plasma length, is simplified when using conclusion [18] that the results of numerical modeling of axial distributions of parameters are close to the results of their analytical calculation based on the cylindrical explosion theory [21]; the flow of laser plasma downstream LSDW front is isentropic in the asymptotic region. The results of analytical calculations of jet flow parameters at a relatively small distance from LSDW front, except for $z < 0.1$, approach the numerical solution; in the asymptotic region, the error does not exceed 10 %. As a result, axial distributions of the flow parameters — enthalpy, density, velocity — can be determined from the relations

$$h/h_w = (p/p_w)^{(\gamma-1)/\gamma},\ \rho/\rho_w = (p/p_w)^{1/\gamma},$$

$$u^2 + 2h = u_w^2 + 2h_w. \quad (4)$$

The flow velocity $u$ is determined in the coordinate system moving at a rate $V$ of LSDW front; the subscript $w$ used corresponds to the plasma conditions right downstream the front, which for the detonation wave are determined by the relations

$$\frac{\rho_W}{\rho_\infty} = \frac{\gamma+1}{\gamma}, \quad \frac{\rho_W}{\rho_\infty V^2} = \frac{1}{1+\gamma},$$

$$\frac{u_W}{V} = \frac{c_W}{V} = \frac{\gamma}{1+\gamma}, \quad \frac{h_W}{V^2} = \frac{\gamma^2}{(\gamma+1)^2(\gamma-1)}. \quad (5)$$

The velocity of the front when moving towards the beam is determined by the expression [6]:

$$V = [2(\gamma^2-1)q/\rho_\infty]^{1/3}, \quad (6)$$

where intensity of the laser beam $q = W/s$, $W$ — absorbed power and $s = \pi r_0^2$. The effective value of the ratio of specific heat in highly ionized plasma $\gamma$ is $\sim (1.2 \pm 0.05)$.

The radius $r$ of the jet flow is estimated from the continuity equation for a sufficiently uniform flow expressed as

$$\rho u r^2 = \rho_w u_w r_0^2 = \rho_\infty V r_0^2. \quad (7)$$

The relative velocity of the jet flow in the environment is $u_x = (u - V) > 0$, increasing to $u_x \approx 1/2V$ as moving away from the front [18].

As part of the analytical approach, nonstationary solutions of the point cylindrical explosion model are used to determine the jet parameters [21]:

$$r(t) = \left(\frac{E_0}{\alpha\rho}\right)^{1/4} t^{1/2},$$

$$p_2 = \frac{2}{(\gamma+1)}\rho\left(\frac{dr}{dt}\right)^2 = \frac{\rho}{2(\gamma+1)}\left(\frac{E_0}{\alpha\rho}\right)^{1/2} t^{-1}. \quad (8)$$

$p_2(t)$ determines the surge pressure — at LSDW front, and radius $r(t)$ — defines the boundary of the contact surface downstream the front. In the heavy explosion theory, the pressure $p$ in the central area of the explosion stabilizes in magnitude for a short time and accounts for a certain portion $\beta$ of the surge pressure, i.e. $p = \beta p_2$. The degree of pressure reduction depends on the properties of gas and, for example, makes $\beta = 0.442$, 0.426 and 0.441 at $\gamma = 1.15$, 1.2 and 1.25, respectively. The dimensionless parameter $\alpha = E_0/E$ used in the heavy explosion model determines the relationship between the energy parameter $E$ and the amount of energy $E_0$ per unit length of the cylindrical explosion, so that $E_0 = \alpha E$. This parameter depends on gas properties and rises during subsidence of $\gamma$. According to data from [21] parameter $\alpha = 2$ at $\gamma = 1.2$, when $\gamma$ varies within $\pm 0.05$ the changes of $\alpha$ approach 0.5. Further, for estimates we used values $\alpha = 2.5$ at $\gamma = 1.15$ and $\alpha = 1.5$ at $\gamma = 1.25$.

Next, using the expressions (6) and (8), as well as the relationship of the energy parameters of both models $E_0 = qs/V = q\pi d^2/(4V)$, we obtain

$$\left(\frac{E_0}{\alpha\rho}\right)^{1/2} = \left[\frac{\pi}{8\alpha(\gamma^2-1)}\right]^{1/2} Vd. \quad (9)$$

As a result, taking into account (5), (8) and (9), we determine the axial pressure distribution, which takes the following form:

$$p(z)/p_w = K_p(\gamma+1)z^{-1},$$

$$K_p = \left[\frac{\beta}{2(\gamma+1)}\right]\left[\frac{8\alpha(\gamma^2-1)}{\pi}\right]^{-\frac{1}{2}}. \quad (10)$$

As noted above, (10) takes into account a decrease in pressure in the center of the explosion using coefficient $\beta = p/p_2$, which is much weaker than parameter $\alpha$ and depends on the properties of the environment. After that from (4), (10) other parameters of the jet flow downstream the LSDW front are determined:

$$\frac{\rho}{\rho_\infty} = K_\rho z^{-1/\gamma},\ K_\rho = [K_p(\gamma+1)]^{\frac{1}{\gamma}}\left(\frac{\gamma+1}{\gamma}\right) \quad (11)$$

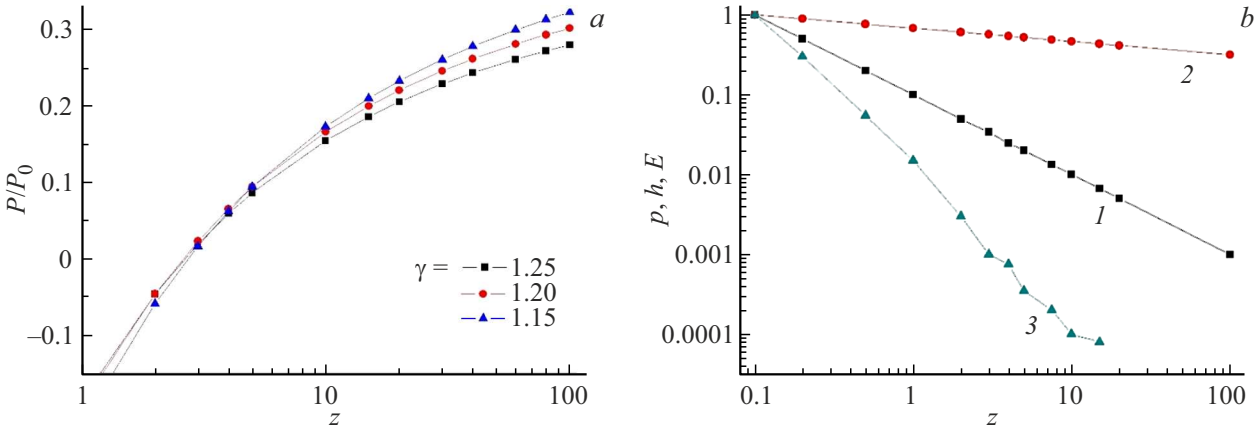


**Figure 1.** Relative magnitude of pulse $P/P_0$ depending on the distance $z$ ($a$); parameters of plasma: *1* — pressure, *2* — enthalpy, *3* — radiation downstream LSDW front ($b$).

$$\frac{u}{V} = \gamma \left[\frac{(\gamma-1)}{(\gamma+1)}\right]^{\frac{1}{2}} [1 - K_u z^{(1-\gamma)/\gamma}]^{\frac{1}{2}} - 1,$$

$$K_u = [K_p(\gamma+1)]^{\frac{(\gamma-1)}{\gamma}} \left(\frac{2}{\gamma+1}\right) \qquad (12)$$

$$\frac{r}{d} = 0.5 \left[\frac{(\gamma-1)}{(\gamma+1)}\right]^{1/4} [K_p(\gamma+1)]^{-\frac{1}{2\gamma}} [1 - K_u z^{(1-\gamma)/\gamma}]^{-\frac{1}{4}} z^{\frac{1}{2\gamma}}. \qquad (13)$$

The relative velocity $u(x)/V$ of the plasma flow in a fixed coordinate system is taken into account in (12) by the second term, in contrast to (5), (7), where this parameter is determined in a frame of reference moving with the velocity of LSDW front. Note that near the front ($z = 0-0.2$), these solutions strongly deviate from the monotonous nature of the change and their values (5) at LSDW front. In this narrow range, linear approximation of solutions up to these values was used.

The obtained solutions (10)–(13) were used in (3) to calculate the relative magnitude of the amount of motion or pulse of the plasma $K = P/P_0$ with the value $P_0 = \rho_\infty V$. The dependence of this parameter on the relative distance $z$ is shown in Fig. 1, $a$. The range of plasma-specific heat ratios $\gamma = 1.15-1.25$ was used with corresponding changes in the coefficients $\alpha(\gamma)$ and $\beta(\gamma)$ in the theory of a heavy cylindrical explosion. The desired parameter depends rather weakly on the ratio of the specific heat of the plasma and increases intensively at low $z$. At $z < 1$ , the flow velocity according to (12) is even less than that of LSDW front ($u/V < 1$), and the needed parameter has a negative value. However, this area is small, and its contribution to the calculation is insignificant; at relative distances $z > 10$, the pulse acquired by the plasma approaches the value $P/P_0 \approx 0.3$.

Fig. 1, $b$ also illustrates the axial distributions of enthalpy and pressure downstream LSDW front, obtained from the appropriate solutions (4), (10). In the experiment at the peak absorption power of $W = 40.2$ kW and beam diameter of $d_0 \approx 0.15$ mm the power density is expressed as the value $q = W/s \approx 2.0 \cdot 10^{12}$ W/m$^2$. LSDW front propagation velocity is $V \approx 9$ km/s. Accordingly, the pressure and specific enthalpy downstream its front increase to $p_w \approx 770 \cdot 10^5$ Pa and $h_w \approx 120$ MJ/kg at the initial pressure in the subsonic argon stream of $p_\infty = 10^5$ Pa. Pressure (1) decreases significantly already at a short distance from the front, while the enthalpy (2) decreases significantly less, no more than 50,% at large distances. Accordingly, the temperature of plasma goes down — from $T = 42$ kK near the front to $T = 21$ kK at a distance of $x = 10d$ ($z = 10$). With further increase of distance the temperature of plasma varies less intensely, e.g., $T = 19$ kK ($z = 20$) because of poor change of enthalpy.

The credibility of the obtained results depends on the degree to which the assumptions used are fulfilled: uniform distribution of power density over a cross-section of a beam of constant diameter, constant power level of the laser pulse. The use of stationary ($V = \text{const}$) solutions (10)–(13) also implies a fast determination of these parameters compared to the duration of the laser pulse. In real conditions, these terms are not completely fulfilled, which can lead to a noticeable change in the parameters of the amount of plasma motion, respectively. In addition, the distribution of parameters may be affected by plasma energy losses due to radiation yield. First, it is necessary to determine the qualitative role of radiation — its strong or weak impact on the plasma parameters downstream LSDW front.

### 1.2. Energy balance of plasma and role of radiation

The role of radiation is estimated by the ratio of specific energy parameters, [W/m$^3$], — spectrum-integral radiation losses of plasma relative to the power absorbed by the plasma. The value of the first parameter $E_{rad} = 4\pi\varepsilon$ may be estimated using the ratio given in [22] for calculating the spectrum-integral radiation flow of an optically thin plasma, obtained on the basis of the principle of spectroscopic stability and taking into account the results of experiments

with argon plasma of continuous optical discharge:

$$\varepsilon = C_R \left[\frac{T}{10^4}\right]^{\frac{1}{2}} \exp^{-\Delta I/kT} N_e[N_+ \exp(h\nu_g/kT) + 2^2 N_{++} \exp(h\nu_g^+/kT)]. \quad (14)$$

Here, the constant $C_R = 1.14 \cdot 10^{-39}$ W/(m$^3$·sr), $T$ — temperature, $N_e$, $N_+$, $N_{++}$ — concentrations, [m$^{-3}$], electrons, ions, single- and double ionization, $\Delta I$ — reduction of ionization potential, $h\nu_g$ and $h\nu_g^+$ — decrease of energy boundaries of continuous spectra for atoms and ions — 2.85 and 8.2 eV respectively. Using the new energy boundaries of the continuous spectrum, the multiplier $\exp h\nu_g/kT$ takes into account the contribution of linear radiation, or pseudocontinuum. Thus, the calculation of the ratio (14) takes into account the spectrum integral recombination, braking, and also, approximately, radiation in the lines. In addition, the values of charged particle concentrations necessary for calculating were obtained using systematized data from tables of thermodynamic parameters of argon [23].

The curve *3* in Fig. 1, *b* shows that the local radiation flow $E_{rad} = 4\pi\varepsilon$ undergoes even higher decrease than pressure by — by 4 orders of magnitude as it moves away from the front in the range $z = 0.1-10$. Integration of the distribution $E_{rad}(z)$ over the volume of the micro-jet within $z = 0.1-15$, taking into account changes in its cross-section, shows that a layer with a thickness of $5d$ emits more than 90 % of the total flow. Consequently, the main part of the total radiation flow of LSDW plasma comes out of a narrow layer downstream the front, where a high temperature is kept. Then this parameter decreases to values in the range $T = 21-19$ kK; it will continue to decrease when the power supply is stopped.

In the model used, the condition for the existence of the LSDW mode is the absorption of the dominant part of the laser power $W$ in a narrow $\delta \ll d_0$ thick layer, i.e. in its volume $v = s\delta$. To determine the specific — per unit volume — plasma-absorbed power we use the above-mentioned estimate of the power density $q = W/s \approx 2.0 \cdot 10^{12}$ W/m$^2$. Therefore, the specific value [W/m$^3$], of the plasma-absorbed power $E_{absorp} = W/v = q/\delta$. It follows from the necessary condition for the existence of LSDW mode that the layer thickness is $\delta \leq 0.1d_0$. Even with the overestimated $\delta = 0.5d_0$ ($d_0 = 0.15$ mm) it turns out that under peak absorption the value $E_{absorp} \approx 26.7 \cdot 10^{15}$ W/m$^3$, which is by over 12 times higher than the maximum of the radiation flow from plasma $E_{rad} = 2 \cdot 10^{15}$ W/m$^3$. The portion of radiation losses in the total plasma energy balance, even with an overestimation, is $E_{rad}/E_{absorp} \leq 0.08$, which indicates a weak effect of radiation energy losses on the parameters of the plasma breakdown downstream LSDW front under starting conditions.

When the velocity decreases until LSDW stops ($V \leq 4$ km/s), the role of radiation is estimated in a similar way. Pressure and enthalpy on the front are decreased proportionally to $V^2$ respectively $p_w \approx 152 \cdot 10^5$ Pa, $h_w \approx 23.7$ kJ/g, also $T \approx 18$ kK. The plasma radiation power decreases by more than two orders of magnitude, while the absorption power of $E_{absorp}$ decreases by no more than 5 times, as follows from the measurement results of the absorption pulse. Hence, the portion of radiation in the general energy balance of plasma$E_{rad}/E_{absorp}$ is significantly lower compared to its initial ($< 8$ %) value. A similar conclusion about the weak effect of radiation energy losses on plasma parameters downstream LSDW front is also outlined in papers [19,24], where the role of plasma radiation was evaluated under similar conditions.

Thus, the proposed method for estimating the amount of motion or pulse of plasma laser LSDW is universal due to the absence of an explicit dependence of the flow parameters on the beam diameter and its power. This is because of the interrelation of parameters: $V \propto q^{1/3}$ and $q \propto d^2$. The amount of plasma motion is proportional to the product of two parameters: $P = K\rho_\infty V$ with coefficient $K$, which depends on the length of plasma and intensely grows at low $z$, slightly rising up to$K \approx 0.2-0.3$ in the range $z \approx 10-100$. The desired parameter is almost independent of the ratio of the specific heat of the plasma. In real conditions, especially with short focusing, the value of the coefficient $K$ may change, possibly even rising during unsteady plasma expansion processes with its elevated temperature in the initial stage. Yet, in this paper $K = 0.2$ is used to account for the pulse of plasma LSDW. A comparative analysis of the data from numerical modeling and experiment [15] will make it possible to determine the possibility of using it in the approach used.

## 2. Technique and experimental results

In the work of [15], an optical discharge was initiated by a focused beam of $CO_2$-laser in a subsonic (250 m/s, $M = 0.88$) isobaric argon stream flowing out of a channel with a diameter of 5 mm. Focusing point of laser beam $x = (5 \pm 0.5)$ mm from the channel transect, beam diameter before focusing $D \approx 25-27$ mm, focal distance of lens $F = 254$ mm, which defines the condition of an extended focusing with a parameter $f = F/D \approx 10$. At 40kHz laser pulse repetition rate (period 25,$\mu$s), each discharge was visualized, and no skips were observed. Each discharge corresponded to up to 6 luminescence frames, then it weakened greatly and was not observed until the next discharge, which was recorded in the subsequent twelfth (480 K/40 K) frame.

Fig. 2, *a* in the top shows the first plasma luminescence frame, located within the subsonic flow, below — the following second frame. Plasma luminescence was recorded by a high-speed camera Photron SA-Z within the spectral range of 400−1000 nm, maximum — in the region 700 nm, frame size — $384 \times 64$ pixels. Recording parameters: exposure time 1.0 $\mu$s, shooting frequency 480 kHz, i.e. time interval between the frames — 2.08 $\mu$s. Accordingly, the recording time intervals between the two first frames

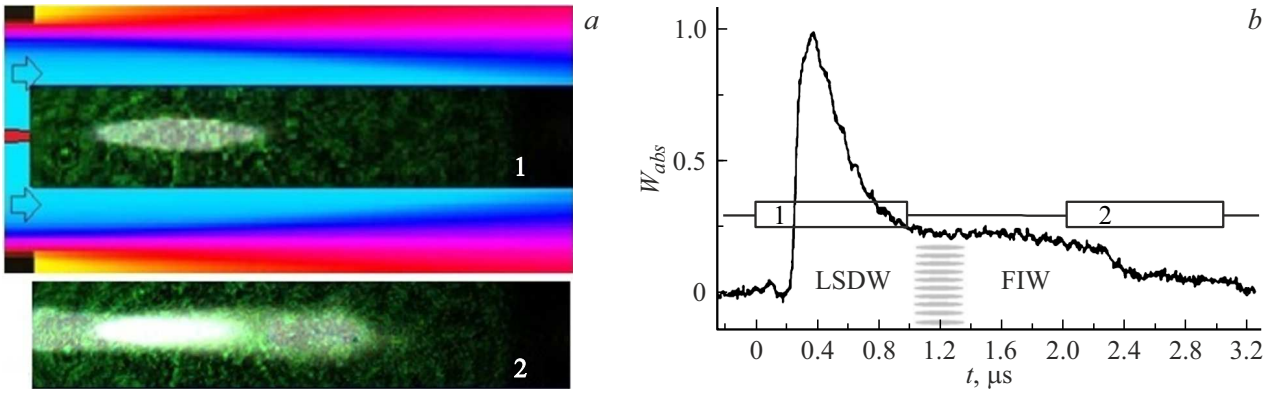


**Figure 2.** Plasma luminescence in the first (top) and second (bottom) frames ($a$); laser pulse absorption profile ($b$). Frame size — $11.5 \times 2$ mm, focusing — 5 mm.

make $0-1.0$ and $2.083-3.083\,\mu$s. At the velocity of the discharge front, for example, 10 km/s, its displacement in the frame is 10 mm, while the displacement by the flow is significantly less — 0.25 mm. Consequently, the high-speed discharge front is recorded in the frame as a luminous extended „trace", significantly exceeding the displacement of the object by the flow. Fig. 2, $b$ shows the measured profile of the absorbed power $W_{abs}(t)$ of a laser pulse against the sequence of the first two $(1, 2)$ frames. The profile is obtained by subtracting the amplitude of the signal transmitted through the plasma from the amplitude of the incident signal (as shown in [15]). At each discharge, the absorption pulse could shift within no more than $1\,\mu$s relative to the frames due to uncontrolled variation of the Q modulator parameters in the laser system [15]. As a result, in part of the data ($\sim 20\,\%$), a two-leaf structure of plasma luminescence was observed in the first frame — a precursor of the short absorption front being located at the end of the first frame exposure time. This precursor appears because a small part of the beam power is passing beyond the focusing point, whereas the intensity of luminescence being also varied due to the variation of the laser pulses amplitude. In the rest portion of the data, the specified condition was not met, and no precursor was observed. But in all cases, the subsequent dynamics of plasma luminescence was identical, which made it possible not to take into account the precursor in the computational model early in the study.

With the laser pulse basic duration of $3.0-3.5\,\mu$s the breakdown on its front is distinguished by a much shorter, no less than $0.1\,\mu$s, duration. Therefore, in the model used, the breakdown stage with its complex of collision-radiation processes of optical discharge plasma formation is not considered. Power of $W_{abs} = 40.2$ kW is maximally absorbed. After the absorption peak area of $0.4-0.45\,\mu$s follows the „plateau" with duration of $\sim 1.5\,\mu$s, with an amplitude of $\sim 0.20$ of its maximum. Each region contains $\sim 1/2$ part of the laser pulse energy.

The peak absorption intensity is estimated at $q \approx 2 \cdot 10^{12}$ W/m$^2$ in a beam with a diameter of 0.15 mm, as already noted in section 1. This parameter is much higher than the threshold value necessary for the fast ionization wave (FIW) to occur with the front velocity in argon of $80-90$ km/s [11,12], which is much higher than that of LSDW front — 9 km/s. Nevertheless, at peak power, LSDW mode is implemented due to the small size of the focus spot, i.e., the primary plasma. LSDW mode stops after peak power due to a decrease in the front velocity to „threshold" values that exclude the existence of this mode [15].

The second frame in Fig. 2, $a$ always shows an extended luminescence region towards the beam. This indicates the effect of UV radiation from the plasma, which excites the surrounding cold gas, followed by its ionization in an IR laser beam, similar to the mechanism of a fast ionization wave. The considerable length of the luminescence region, reaching the nozzle edge and beyond, corresponds to the already noted fact of a high ionization wave velocity. The delay ($\sim 1\,\mu$s) of the priority intensity FIW mode is due to the significant dependence of this mode on the transverse size of the primary plasma, which is insufficient in the initial stage of discharge. However, this parameter increases during the radial expansion of plasma with energy absorption in the area of power „plateau" which keeps the high temperature. The modes change area is shown in Fig. 2, $b$ in the interval of $t = (1.2 \pm 0.2)\,\mu$s. The exact boundary is not determined due to the incomplete identity of the initial experimental conditions due to variations in the amplitude and intensity profile of the laser pulse.

Thus, the data obtain from [15] indicates that LSDW mode of the discharge propagation occurs in the peak of absorption of laser pulse transforming after $\sim 1\,\mu$s into FIW mode in the „plateau" area of the laser pulse with a duration of $\sim 1.5\,\mu$s. In addition to the energy, the volume of LSDW plasma acquires the amount of movement in the direction of the laser beam, and FIW plasma absorbs the remaining $\sim 1/2$ part of the laser pulse energy without forming plasma fluxes in the axial direction.

## 3. Numerical modeling results and discussion of results

### 3.1. Computational model of the energy source taking into account the LSDW and FIW modes

The approach used takes into account the established sequence and the identified features of the propagation modes $CO_2$- of the laser discharge:

1) the duration of the early stage of the appearance of primary electrons is significantly shorter than the total duration of the laser pulse;

2) the velocity of discharge propagation is significantly higher than the characteristic scale of the velocity of gas dynamic disturbances. In addition, taking into account the experimental data that laser plasma luminescence noticeably decreased much later than the laser pulse had been absorbed, energy losses were neglected in the studied characteristic time scale of $0-10\,\mu$s. Nevertheless, this allowed us to determine the effect of the jet flow on the plasma structure.

The computational model uses a system of hydrodynamic equations in which plasma regions are energy (heat) sources having a specific set of space-time parameters, as it has been used in numerous computations [3,4]. The parameters of such a source are determined using experimental data on the behavior of the absorbed power of the laser pulse, the spatiotemporal scales of plasma in the LSDW and FIW modes. In contrast to the generally accepted approach, the value of the integral parameter is additionally used - the amount of motion (momentum) acquired by the LSDW plasma. No directed plasma flow is formed in FIW mode.

The model of the energy source in the axisymmetric subsonic argon flow contains $(1, 2)$ two laser energy absorption regions; the scheme is shown in Fig. 3; the spatiotemporal and energy parameters — are provided in the table. The results of measurements of the plasma length and absorbed energy in these characteristic pulse time intervals are used. In the early stage $0-1\,\mu$s LSDW occurs in the interval of $x = 2-5$ mm (region 1). Plasma pulse $P = KP_0$, where$P_0 = \rho_\infty V$, $K = 0.2$, front velocity $V = 9$ km/s. During the following period $1-2.5\,\mu$s the region of the heat source is enlarged, including 1, varying from $x = -2$ mm to $x = 5$ mm, without formation of directed flows, equivalent of the fast ionization wave mode. The point „0“ of the coordinate system is located on the axis of the flow $0x$, reference point — from the channel edge. The initial transverse size of the source $d = 0.15$ mm is equal to the diameter of the focused beam. Its increase as it moves away from the focus point was neglected, since it has little effect on the calculation result of the radial expansion process. The energy of the source in 1-th region $E_1 = 13$ mJ, which is half of the full pulse energy. In region 2 the remaining portion of energy $E_2 = 13$ mJ is absorbed in the time interval $1-2.5\,\mu$s („plateau“) in both, the earlier formed LSDW plasma

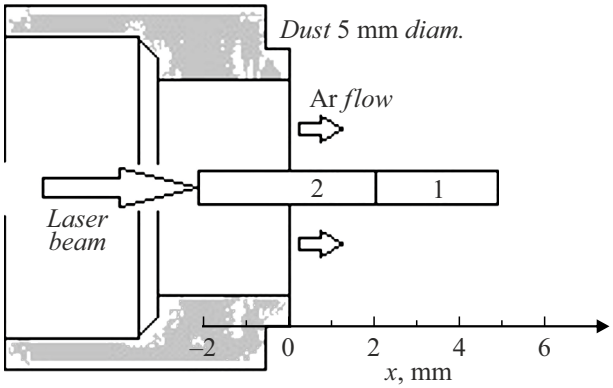


**Figure 3.** Energy source scheme.

downstream the front, and in gas upstream the plasma, i. e within $x = (-2)-(+5)$ mm. At the same time, the question arises about the axial distribution of energy along the beam. Based on the fact that the observed additional luminescence (2-th frame) is fairly uniform along the axis, the same energy distribution is assumed in the second region of the source. The upstream length is not precisely determined, since the leading edge of the luminescence is blocked by the channel. According to the data of subsequent frames, taking into account the flow rate, the increase in the region boundary upstream does not exceed 2 mm. Therefore, in the computational model, this boundary towards the laser beam is increased by 2 mm and is located inside the channel. The results of the control calculation with a reduction of the absorption boundary from $x = -2$ mm to $x = 0$ mm showed no noticeable differences in plasma behavior pattern.

The second version $(b)$ of the computational model differs only in that LSDW mode is neglected $P/P_0 = 0$. A comparison of the results of numerical modeling of the flow structure in the presence of an energy source and a pulse (version $a$) with similar data neglecting the pulse $(b)$ will allow us to draw certain conclusions regarding the possibility of using the proposed approach to modeling laser plasma.

### 3.2. Numerical modeling of laser power supply and data representation

Supply of laser energy with the specified parameters to a subsonic argon flow was numerically simulated for a non-stationary problem in an axisymmetric formulation using ANSYS FLUENT software. The solution area was determined by the geometry of the channel used in the experiments; it included the upper boundary of the channel wall, the lower boundary of the symmetry axis. Left boundary corresponded to the inlet, right boundary — to the outlet of the channel. The computational grid included about 200 thousand tetragonal cells.

The problem was solved in the framework of the Reynolds-averaged Navier-Stokes equations supplemented

Energy source parameters

| Model version | Region | Interval of time, $\mu$s | Coordinates, $x1-x2$ mm | Diameter $d$, mm | Energy $E$, mJ | $P/P_0$ |
|---|---|---|---|---|---|---|
| $a$ | 1 | 0–1 | 2–5 | 0.15 | 13 | 0.2 |
| | 2 | 1–2.5 | (−2)–(+5) | 0.15 | 13 | 0 |
| $b$ | 1 | 0–1 | 2–5 | 0.15 | 13 | 0 |
| | 2 | 1–2.5 | (−2)–(+5) | 0.15 | 13 | 0 |

by the turbulence model $k-\omega$ SST. The FLUENT solver was used with an algorithm for determining pressure from the equation of state of a perfect gas with an implicit Roe scheme of the second approximation accuracy order. The solid wall condition was used as boundary conditions at the upper boundary of the computational domain. The argon conditions in the pre-chamber were set at the input boundary: static pressure $p = 1.8 \cdot 10^5$ Pa, temperature 290 K. The corresponding types of conditions were used on the axis of symmetry and the output boundary. The boundaries of the isobaric flow downstream the channel edge are shown in Fig. 2, *a* top, ts parameters on the axis: density $\rho_\infty = 2.1\,\text{kg/m}^3$, temperature $T = 240$ K, velocity — 250 m/s.

The values of the energy and momentum of plasma LSDW pulse obtained from the experimental data were set by additional terms in the equations of conservation of energy and quantity of motion. For this purpose, a function was written in C programming language that specified the spatiotemporal parameters of the area of the simulated laser plasma, taking into account the characteristics of LSDW and FIW modes. The energy source in each area was determined as a specific value obtained by dividing the energy ($E_1$, $E_2$) by the volume of the energy supply area. The volume was determined based on the length of the plasma and its diameter. In the equation of momentum conservation, the calculated value of the specific force was used as follows: $P_0/\tau$, [N/m$^3$], where the value of LSDW plasma momentum $P_0 = 0.2\rho_\infty V$ $(K = 0.2)$ and duration of the peak power $\tau = 0.4\,\mu$s at which this mode takes place.

The calculation method uses assumptions acceptable for testing this approach: the equation of a perfect gas with enthalpy of the form $h = C_\text{p}T$, the ratio of specific heat $\gamma = 1.67$. Also temperature limitation from the top is introduced: $T \le 15$ kK, since high plasma temperature is realized only in a narrow layer during a short period of LSDW mode, as shown in section 1.2. For comparison, a control calculation was performed with the value $\gamma = 1.3$, characteristic of argon plasma in the range $T = 10-15$ kK. The result showed a slight, no more than a few percent, change in the values of the laser plasma parameters while fully maintaining the characteristic trends in their behavior pattern.

The calculated data on the temperature distribution ($T$-field) were transformed into the corresponding luminescence distribution $S$ in order to compare with the results of recording the plasma luminescence distribution in the experiment. To determine the luminescence, the ratio for the spectral power of plasma radiation is used as outlined in [22].

$$\varepsilon(\nu) = \text{A}Ne_e^2\xi(\nu)T^{-1/2}\exp[h(\nu_g - \nu - \Delta I)/kT], \quad (15)$$

where A = const, $\xi(\nu)$ — a multiplier of the order of one that weakly depends on temperature and takes into account the specific structure of the atomic terms [22].

Radiation signal amplitude or luminosity $S$ are determined through integration (15) in the working frequency band $\nu 1-\nu 2$ of camera FASTCAM in the area of maximum 500–800 nm:

$$\int_{\nu 1}^{\nu 2} \varepsilon(\nu)d\nu = C_F T^{\frac{1}{2}} N_e^2 \xi(\nu)\exp[(h\nu_g - \Delta I)/kT]. \quad (16)$$

Coefficient $C_F$ depends on the shape of sensitivity curve in the working frequency band. Using the ionization equilibrium equation (Saha), we obtain the value $S$ depending on the plasma parameters:

$$S = C_2\rho(1-\alpha)T^2\exp\left[\frac{(h\nu_g - E_i)}{kT}\right]$$
$$= C_2\rho(1-\alpha)T^2\exp\left[\frac{-149.6}{T(kK)}\right]. \quad (17)$$

The coefficient $C_F$ is transformed into $C_2$, taking into account the corresponding physical constants used in Saha equation, and the dimension $T$ into kK. As mentioned above, the high plasma temperature is realized only behind a narrow shear front during a short period of its movement, then the parameter decreases. In the calculated temperature range $T = 15-10$ kK, the degree of plasma ionization $\alpha$ varies by no more than an order of magnitude at the realized pressures, while the temperature function $\exp[-149.6/T]$ varies significantly more. Therefore, the spatial distributions of the relative temperature $T(x, y)/T_\text{max}$ obtained in the calculation are transformed into the relative luminosity field

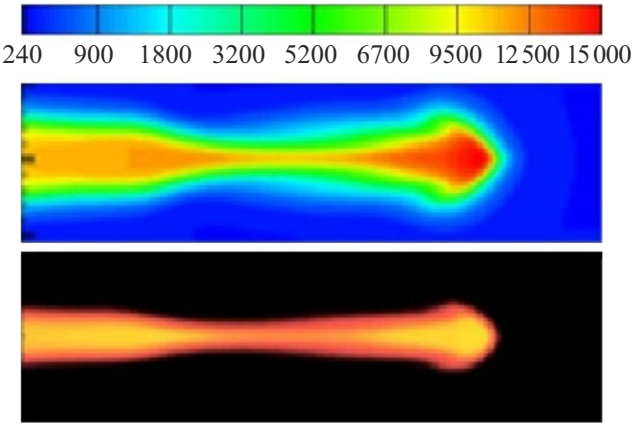


**Figure 4.** $T$ — distribution (top) and $S/S_{\max}$ (bottom); $t = 6\,\mu$s.

$S/S_{\max}$ in the following form:

$$S/S_{\max} = (T/T_{\max})^2(\rho/\rho_{\min}) \times [\exp(-149.6/T)/\exp(-149.6/T_{\max})], \quad (18)$$

where the limiting parameters $T_{\max}$ and $\rho_{\min}$ are realized upon completion of energy absorption ($t = 3\,\mu$s). To compare the primary temperature distributions and the luminosity data transformed by the specified method Fig. 4 illustrates the results of calculation of temperature field (top — temperature scale) and relative luminosity S/Smax at time $t = 6\,\mu$s, taking into account the plasma pulse ($K = 0.2$). The representation of luminosity in FLAME scale shows areas of increased (8–15 kK) plasma medium temperature due to the strong $T$-dependence of the parameter (18).

### 3.3. Data comparative analysis

In the left part of Fig. 5 the results are shown for calculation ($t = 1$, 2, 4, 6, 8 and $10\,\mu$s) of temperature field with energy supply neglecting the plasma pulse ($b$, $P/P_0 = 0$). Right — calculation data accounting for the pulse plasma ($a$, $P/P_0 = 0.2$). Below the calculated data are the luminescence visualization frames in the specified recording time intervals (0–1 $\mu$s, 2.08–3.08 $\mu$s, and etc.) for each frame. In the right the luminescence of the precursor is observed, in the left — no luminescence is observed. The subsequent almost identical dynamics of plasma luminescence is an evidence of a weak effect of the precursor, as already noted in section 2. The modeling and experimental results compared demonstrate that the influence of the plasma pulse is manifested in the formation of a more extensive plasma structure. The head or core is — LSDW plasma, and its trace is caused by the absorption of energy in FIW mode, the energy supply stops after $3\,\mu$s (after the second frame). The head part gets a higher velocity (Fig. 6); and when it „breaks“ the cross-section of the waist is diminished. The influence of the precursor in the picture on the right is not noticeable. Thus, the data obtained show that upon completion of the laser pulse energy absorption, after the second frame, a flow is formed having an increased velocity of the primary LSDW plasma. Note that, in contrast to modeling results, the experiment shows a noticeable decrease in the intensity of plasma luminescence after $\sim 9\,\mu$s due to the growing energy losses. Nevertheless, the data presented in Fig. 5, as well as in the figures below, made it possible to unambiguously establish the effect of the micro-jet flow on the overall plasma structure.

Figure 6 shows the results of calculating the axial distribution of plasma temperature and velocity at various time points. (1, 3, 5, 7, 9 $\mu$s) in a flow with a subsonic velocity of 0.25 km/s. In Fig. 6 in the top — during formation of LSDW plasma, bottom — in the absence of this mode. Micro-jet flow is featuring a high (up to 3.6 km/s) axial velocity in the extended region during (0–3 $\mu$s). Subsequently, the high-speed region expands, and the velocity decreases to 1.1km/s at a time of 9,$\mu$s. In both versions, the temperature reaches its maximum by the end of the laser pulse ($3\,\mu$s), but its value is not determined above the „plateau“ 15 000 K due to the limitation used in the calculation method. Further, the temperature goes down, it goes down more quickly — when LSDW mode takes place. At the same time, the length of the high-temperature region increases, and the tendency towards the formation of two maxima also rises, and at the beginning of the process it is higher downstream, but later ($\sim 7\,\mu$s) it decreases sharply, the higher temperature remains in the region of another maximum with coordinates close to the position of the energy supply area at the peak of the laser pulse. A similar tendency of two luminescence maxima formation is observed in the experiment.

Significant differences in the wave structure formation process can be seen in the absence of LSDW mode (Fig. 6, below). In the region (1), two diverging waves of short, no more than 1 mm, length are formed, faster — up to 800 m/s — in the direction of the flow and the reverse, which is slowed down by the external flow. When the next stage of energy supply is over (region 2, interval 1–2.5 $\mu$s) the waves of various intensity are formed in direct and reverse directions. The velocity of the plasma boundary decreases downstream, and at $t < 9\,\mu$s it becomes balanced with the flow rate.

Also, the obtained radial distributions of the considered parameters showed that the diameter of the high-temperature region along the base is no more than 1.4 mm, and the high-speed region — does not exceed 1.0 mm. For comparison, estimates of the maximum radius of a region of high temperature and low density as per the point explosion theory give the following results: 0.65 and 0.85 mm after $5\,\mu$s for the cylindrical and spherical geometry of the energy source.

The results of the luminosity calculation $S$ show that in the absence of LSDW mode, the area of increased temperature downstream is limited by the coordinate $x < 5$–6 mm

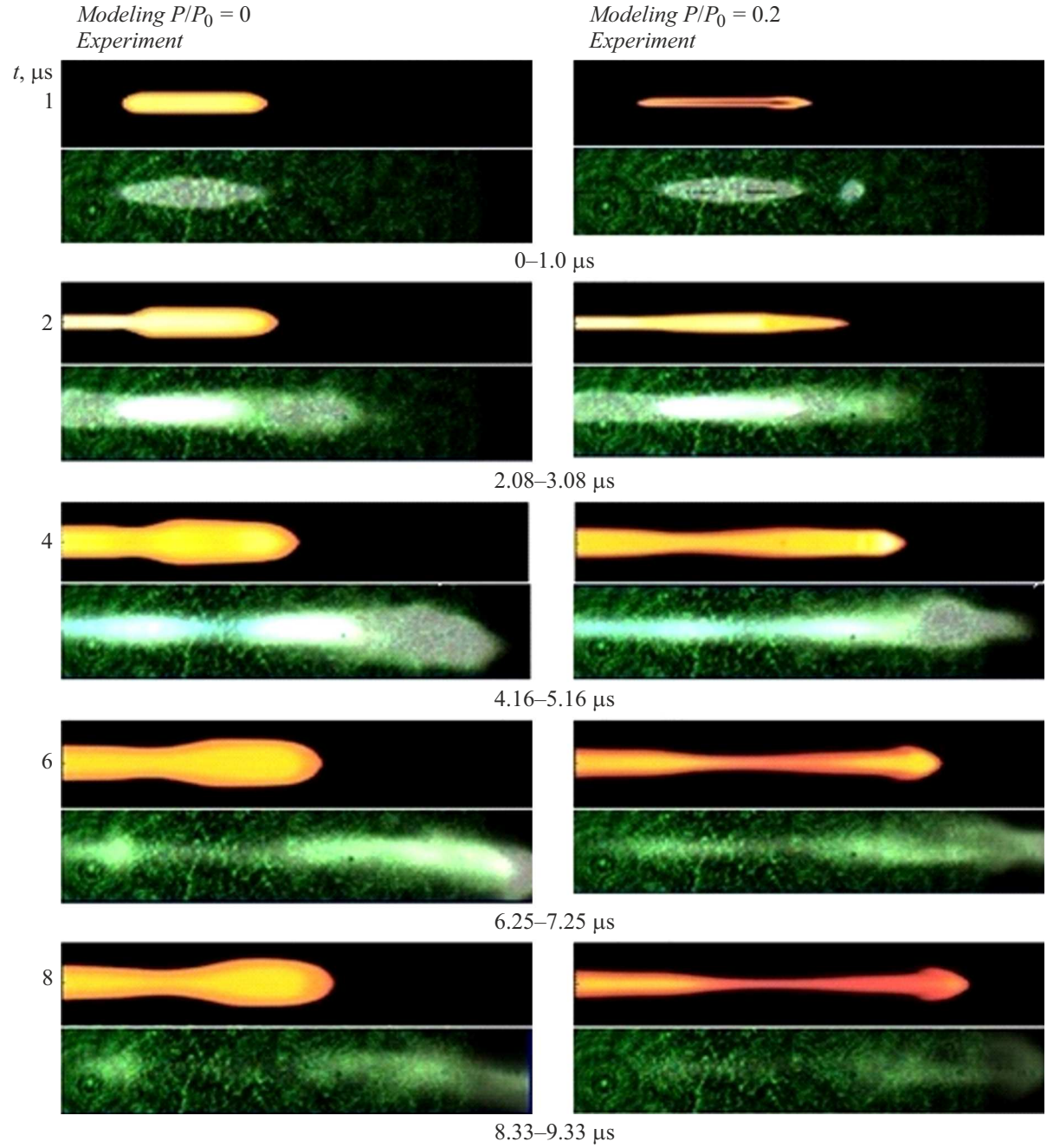


**Figure 5.** Plasma luminescence behavior pattern: modeling, experiment. Frame $11.5 \times 2$ mm.

($t = 9\,\mu$s), while when implemented, there is a noticeable, almost twofold increased shift of this boundary — to $\sim 10$ mm. The effect of the increased axial velocity of LSDW plasma is manifested. The luminosity imaging results also indicate a noticeable, close to calculated, displacement of the plasma boundary downstream.

As mentioned above (sec 3), in experiment jcite15 the luminescence structure of the primary plasma with a precursor was also recorded. This is due to the passage of the laser beam beyond the focus point, similar to the data from the study jcite16 using short-wavelength lasers. The images shown in Fig. 7 illustrating the luminescence of plasma of three different discharges 1, 2 and 3 demonstrate that the precursor plays a certain role in behavior of $CO_2$-laser plasma. The experimental data are presented in the left $(1, 2)$ and right $(3)$ columns, for comparison, in the right column above the discharge images $(3)$, the calculated luminescence distributions previously shown in Fig. 5 are also presented, taking into account the plasma pulse. The recording time intervals the same for all images ($0-1\,\mu$s, $2.08-3.08\,\mu$s and etc.) are shown below in the left, and the time of rated luminescence distribution $t = 1$, 2, 4, 6 and $8\,\mu$s — is shown in the right.

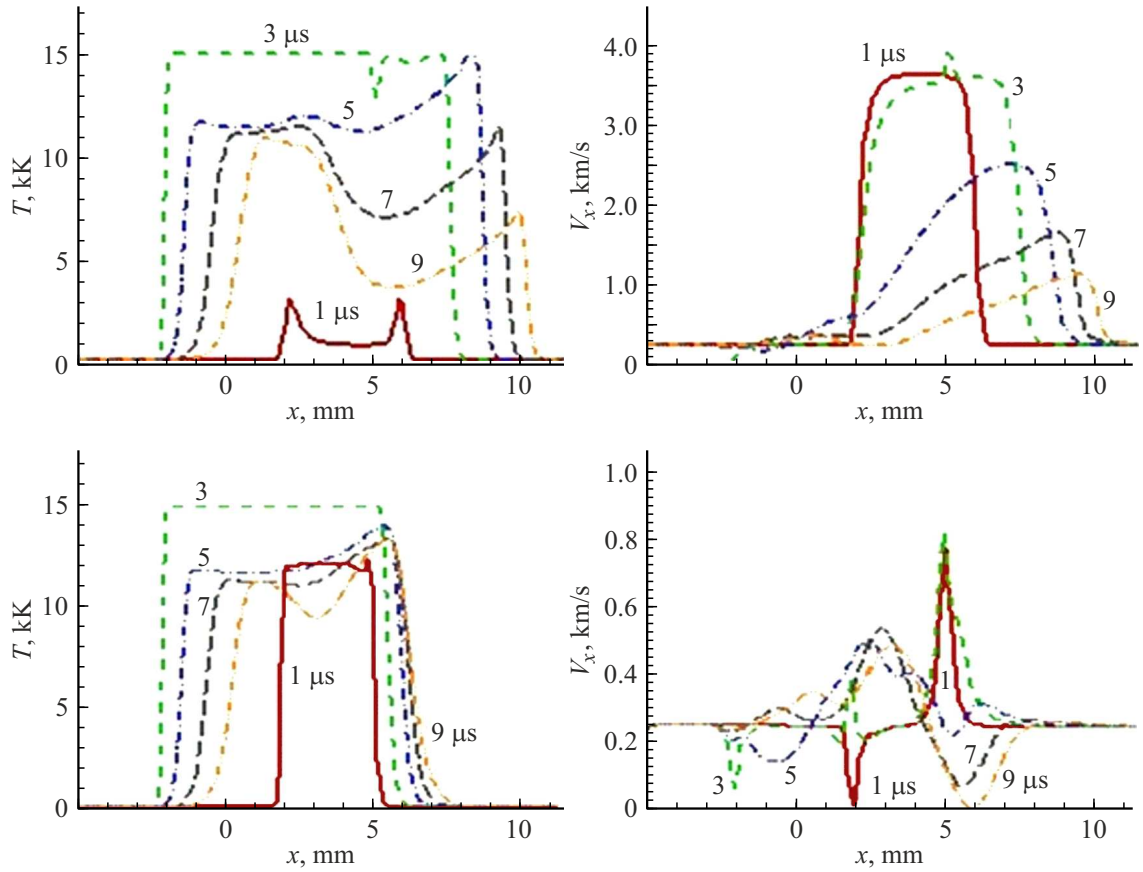


**Figure 6.** Axial distributions of temperature $T$ and longitudinal component of velocity $V_x$ of laser plasma. $P/P_0 = 0.2$ (top), $P/P_0 = 0$ (bottom).

The experimental data in Fig. 7 demonstrate the nature of perturbation of the plasma flow structure when part of the energy is absorbed in a precursor with different luminescence intensity and its position in front of the main plasma. A characteristic trend is revealed: an increase in the radial expansion of plasma with an increase in the chaotic inhomogeneity of the luminescence downstream the precursor, after $2-3\,\mu$s (second frame). It can be assumed that this is due to the interaction of the micro-jet with a region of reduced density in the precursor. Nevertheless, the plasma structure retains the same general appearance as with small perturbations, for example, as in Fig. 5. This also suggests that a relatively small portion of the peak energy of the laser pulse is absorbed in the precursor. To obtain quantitative data using the numerical modeling method, it is necessary to perform a parametric analysis using additional parameters of the precursor: energy, length, position, in comparison with the experimental results. In addition, given the increased disturbances, three-dimensional modeling using appropriate turbulence models is required. Conducting such an analysis is a separate research, which was not included in the scope of this work.

## Conclusion

An approach has been developed and numerical modeling of the behavior pattern of an optical discharge plasma upon absorption of a $CO_2$-laser pulse has been performed. The new approach uses a system of hydrodynamic equations where the modes of propagation of optical discharges are formalized in relation to experimental conditions [15]. Plasma regions are energy (heat) sources with parameters that are determined using experimental data on the behavior pattern of laser pulse energy absorption and the spatial scale of plasma in LSDW and FIW modes. In contrast to the generally accepted approach, the value of the integral parameter is used in the momentum conservation equation — the amount of motion acquired by LSDW plasma. The calculation uses assumptions that are of no fundamental importance in the operating temperature range, which made it possible to use the version of ANSYS FLUENT software in a relatively simple way for a non-stationary problem in the axisymmetric formulation.

The results of numerical modeling show the formation of a more extended plasma structure when taking into account the micro-jet plasma flow in LSDW mode of optical

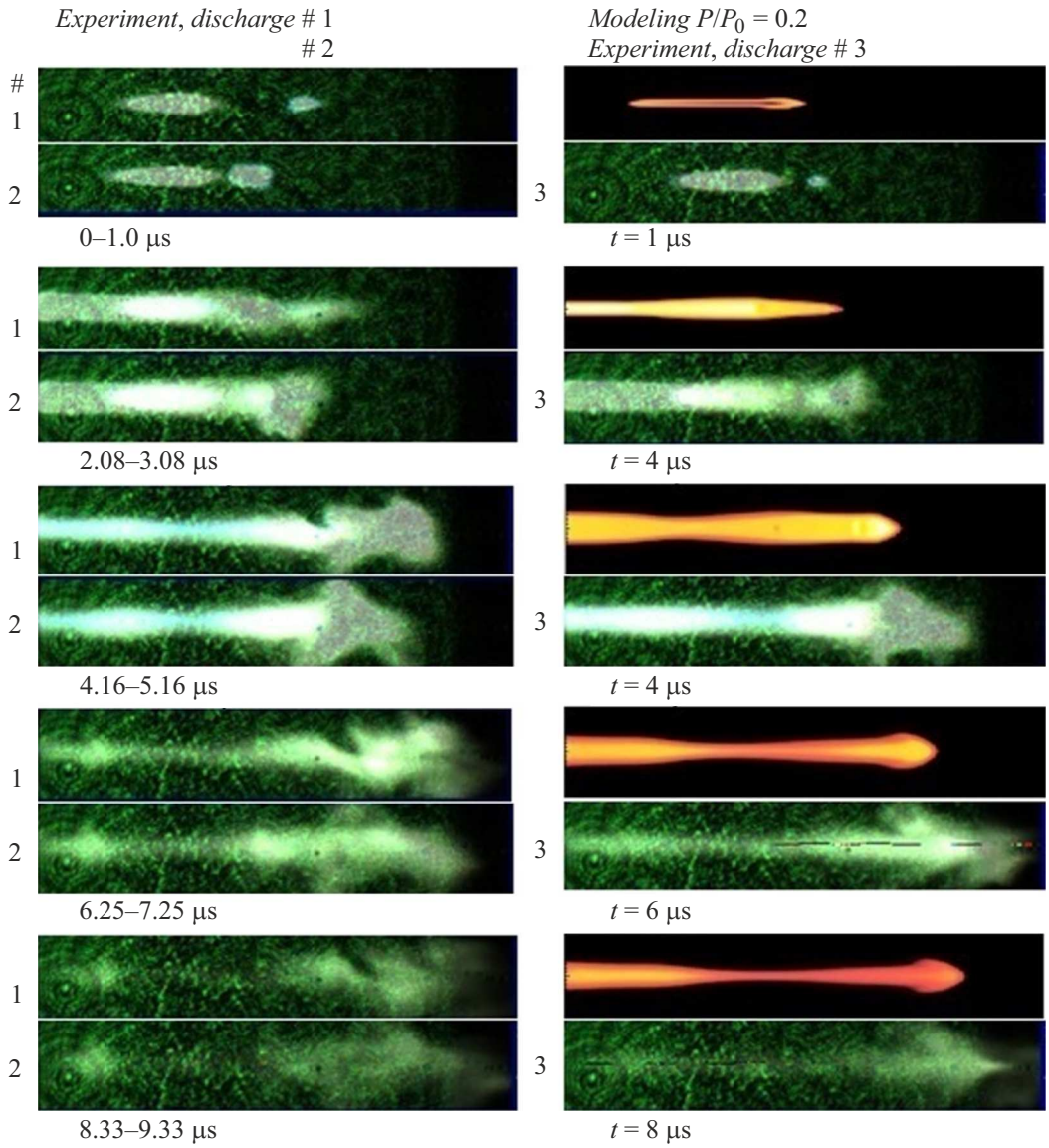


**Figure 7.** Luminescence of plasma with precursor.

discharge propagation. Visualization of luminescence shows a displacement of the plasma boundary downstream, which is close to numerical results. This indicates the possibility of using the calculated value of the integral parameter — the amount of plasma LSDW motion. Numerical modeling also made it possible to determine the characteristic trends in the behavior of plasma structure and parameters. The velocity and temperature reach their maximum values when the absorption of the laser pulse is completed. Subsequently, plasma is separated ahead of its head portion downstream due to the increased velocity of the plasma flow behind the LSDW front. Thus, for the first time in a comparative analysis of the results of numerical modeling and experimental data, the formation of a high-speed micro-jet plasma flow in LSDW mode of optical discharge propagation is confirmed.

### Funding

The study was carried out under the state assignment by RAS SB ITAM (state registration number: 124021400036-7, 124021500012-0.

### Conflict of interest

The authors declare that they have no conflict of interest.

## References

[1] V.A. Bityurin, V.E. Fortov (ed.). *Entsiklopediya nizkotemperaturnoi plazmy*. Series B Thematic volume IX–4. *Plasmennaya aerodinamika* (Yanus-K, M., 2014)

[2] A.S. Yuryev, S.Yu. Pirogov, E.V. Ryzhov. *Upravlenie obtekaniem tel s ispolozovaniem podvoda lasernoy energii v vysokoskorostnye potoki gasa* (Professional, SPb, 2005)
[3] P.Yu. Georgievskij, V.A. Levin. Pis'ma v ZhTF, **14** (8), 684 (1988) (in Russian).
[4] V.N. Zudov, P.K. Tretyakov, A.V. Tupikin, V.I. Yakovlev. MZhG, **5**, 140 (2003) (in Russian).
[5] V.M. Fomin, V.I. Yakovlev. *Energoobmen v sverkhzvukovykh gasoplasmennykh techeniyakh s udarnimy volnami* (Fizmatlit, M., 2017)
[6] Yu.P. Raizer. ZhETF, **48** (5), 1508 (1965) (in Russian).
[7] V.I. Fisher. ZhTF, **53** (11), 2148 (1983) (in Russian).
[8] V.I. Fisher. ZhTF, **53** (11), 2143 (1983). (in Russian)
[9] V.I. Fisher, V.M. Kharash. JETP, **55** (3), 439 (1982).
[10] V.I. Fisher, V.M. Kharash. JETP, **56** (5), 1004 (1982).
[11] K. Shimamura, K. Matsui, J.A. Ofosu, I. Yokota, K. Komurasaki. Appl. Phys. Lett., **110**, 134104 (2017). https://doi.org/10.1063/1.4979646
[12] K. Shimamura, I. Yokota, Sh. Yokota. J. Appl. Phys., **126**, 243304 (2019). https://doi.org/10.1063/1.5115815
[13] K. Mori, K. Komurasaki, Y. Arakawa. J. Appl. Phys., **92**, 5663 (2002). https://doi.org/10.1063/1.1513869
[14] K. Mori, K. Komurasaki, Y. Arakawa. Appl. Phys. Lett., **88**, 121502 (2006). https://doi.org/10.1063/1.2183812
[15] V.I. Yakovlev, V.B. Shulyat'ev, M.A. Yadrenkin, T.A. Gimon. Bull. Lebedev Phys. Institute, **50** (10), S1108 (2023). https://doi.org/10.3103/S106833562322013X
[16] A. Alberti, A. Munafo, M. Koll, M. Nishihara, C. Pantano, J.B. Freund, G.S. Elliott, M. Panesi. J. Phys. D: Appl. Phys., **53**, 025201 (2020). https://doi.org/10.1088/1361-6463/ab492a
[17] S.Y. Pirogov, D.G. Belyanin, A.S. Yuriev, S.V. Leonov, E.V. Ryzhov. Proc. of the 7th Int. *Workshop on Magneto-Plasma Aerodynamics*. Ed. V.A. Bityurin (Moscow, 122-127, 2007)
[18] P.D. Thomas. AIAA J., **15** (10), 1405 (1977).
[19] V.N. Anisimov, V.A. Vorobyov, V.G. Grishina, O.N. Derkach, M.F. Kanevsky, A.Yu. Sebrant, M.A. Stepanova, S.Yu. Chernov. Quant. Electron., **25** (8), 831 (1995). DOI: 10.1070/QE1995v025n08ABEH000481
[20] T.A. Kiseleva, T.A. Korotaeva, V.I. Yakovlev. Tech. Phys. Lett., **45** (4), 335 (2019). DOI: 10.1134/S1063785019040059
[21] L.I. Sedov. *Metody podobia i razmernosti v mekhanike* (Nauka, M., 1987) (in Russian).
[22] G.I.Kozlov, V.A.Kuznetsov, V.A.Masyukov. ZhETF, **66** (3), 954 (1974) (in Russian).
[23] G.I. Kozlov, E.P. Stupitsky. *Tablitsi termodynamicheskikh parametrov argona i ksenona za padayuschei i otrazhennoy volnoi* (IPM AS USSR, M., 1969) (in Russian).
[24] V.I. Yakovlev. Pis'ma v ZhTF, **27** (9), 13 (2001) (in Russian).

*Translated by T.Zorina*